PCCP

COMMUNICATION

View Article Online
View Journal | View Issue

Cite this: *Phys. Chem. Chem. Phys.*, 2014, **16**, 20382

Received 20th May 2014,
Accepted 5th August 2014

DOI: 10.1039/c4cp02201g

www.rsc.org/pccp

New understanding of the difference of photocatalytic activity among anatase, rutile and brookite TiO_2

Jinfeng Zhang,[ab] Peng Zhou,[a] Jianjun Liu[b] and Jiaguo Yu*[a]

In general, anatase TiO_2 exhibits higher photocatalytic activities than rutile TiO_2. However, the reasons for the differences in photocatalytic activity between anatase and rutile are still being debated. In this work, the band structure, density of states, and effective mass of photogenerated charge carriers for anatase, rutile and brookite TiO_2 are investigated by the first-principle density functional theory calculation. The results indicate that anatase appears to be an indirect band gap semiconductor, while rutile and brookite belong to the direct band gap semiconductor category. Indirect band gap anatase exhibits a longer lifetime of photoexcited electrons and holes than direct band gap rutile and brookite because the direct transitions of photogenerated electrons from the conduction band (CB) to valence band (VB) of anatase TiO_2 is impossible. Furthermore, anatase has the lightest average effective mass of photogenerated electrons and holes as compared to rutile and brookite. The lightest effective mass suggests the fastest migration of photogenerated electrons and holes from the interior to surface of anatase TiO_2 particle, thus resulting in the lowest recombination rate of photogenerated charge carriers within anatase TiO_2. Therefore, it is not surprising that anatase usually shows a higher photocatalytic activity than rutile and brookite. This investigation will provide some new insight into understanding the difference of photocatalytic activity among anatase, rutile and brookite.

1. Introduction

In order to solve the increasingly serious environmental and energy crises, the development of highly active heterogeneous photocatalysts has attracted a great deal of attention in recent years. Many investigations are mainly focused on semiconductor-based photocatalysts for pollutant degradation[1–4] and water splitting[5–7] under ultraviolet or visible-light irradiation. Among various oxide and non-oxide semiconductor photocatalysts, titanium dioxide (TiO_2) has been proven to be the most suitable for wide environmental and energy applications because of its suitable valence band and conduction band positions, long-term stability, non-toxicity, cost-effectiveness and strong oxidizing power. In nature, TiO_2 has three polymorphs, namely, anatase, rutile and brookite.[8] Rutile is the stable phase, while the anatase and brookite are metastable phases. Due to difficulty in synthesis, brookite is rarely reported as a photocatalyst.[9] Generally, anatase displays much higher photocatalytic activities than both rutile and brookite.[10–12] However, the detailed physical mechanism and factors affecting the activity difference among anatase, rutile and brookite is still under debate.

Usually, the photocatalytic activity of TiO_2 is strongly dependent on its phase structure, crystallite size, specific surface areas, and pore structure.[13] Although anatase has lower absorbance ability towards solar light than rutile due to the larger band gap (3.2 eV) than that (3.0 eV) of rutile, the photocatalytic activity of anatase is obviously superior to that of rutile. The previous explanation is due to the anatase having a higher surface adsorption capacity to hydroxyl groups and a lower charge carrier recombination rate than rutile.[14,15] The lower photocatalytic activity of rutile is also related to its larger grain size,[16,17] lower specific surface areas and having a worse surface adsorption capacity.[2,18] In addition, the lifetime of photogenerated electrons and holes in anatase is about an order of magnitude larger than that of photogenerated electrons and holes in rutile, thus greatly enhancing the chance of photoexcited electrons and holes in anatase participating in surface chemical reactions.[10] Moreover, the electronic structures of photocatalysts and effective mass of photogenerated charge carriers have a significant influence on the transfer, separation and mobility of photogenerated electron and hole pairs.[19,20] Therefore, an investigation on the electronic structures and effective mass of photocatalysts is very important for understanding the difference in the photocatalytic performance among anatase, rutile and brookite TiO_2. However, to our knowledge, not much research has been reported on the effect of effective mass of photogenerated charge carriers on the photocatalytic activity of anatase, rutile and brookite TiO_2.

[a] *State Key Laboratory of Advanced Technology for Materials Synthesis and Processing, Wuhan University of Technology, Wuhan 430070, P. R. China. E-mail: jiaguoyu@yahoo.com; Fax: +86-27-87879468; Tel: +86-27-87871029*
[b] *Department of Physics and Electronic Information, Huaibei Normal University, Anhui, Huaibei 235000, China*

Herein, we, for the first time, explain the difference of photocatalytic performance among anatase, rutile and brookite TiO_2 according to the differences in effective mass size of the photogenerated charge carriers. The crystal structures, band structures, density of states (DOS), and the partial density of states (PDOS) of anatase, rutile and brookite TiO_2 were calculated by first-principles density functional theory (DFT). Based on the results calculated above, the lifetime and effective mass of photogenerated electrons and holes for anatase, rutile and brookite TiO_2 were discussed to explain their photocatalytic activity differences. This work will provide some new insight into the difference in photocatalytic activity among anatase, rutile and brookite TiO_2.

2. Computational details

All DFT calculations in the present work were performed by CASTEP code based on the plane-wave pseudopotential method.[21] The generalized gradient approximation (GGA) with the Perdew–Burke–Ernzerhof (PBE) was used as the exchange–correlation function.[22,23] The ultrasoft pseudopotential was used to describe the interaction between the ionic core and valence electrons. The lattice parameters and atomic coordinates were relaxed using the cutoff of 550 eV and Monkhorst–Pack grids of $8 \times 8 \times 5$ *k*-points for anatase, $7 \times 7 \times 9$ for rutile, and $5 \times 7 \times 7$ for brookite. Geometric optimization was achieved by using convergence thresholds of 1.0×10^{-5} eV per atom for total energy, 0.03 eV $Å^{-1}$ for maximum force, 0.05 GPa for pressure, and 0.001 Å for maximum displacement. The self-consistent calculations were performed with a total energy convergence tolerance of less than 1.0×10^{-6} eV per atom. The valence electrons were taken into account for TiO_2 corresponding to Ti: $3s^2 3p^6 3d^2 4s^2$ and O: $2s^2 2p^4$, while the remaining electrons were kept frozen as core states. In order to confirm the accuracy of the calculations, the higher cutoff energy and bigger *k*-points were adopted, the results indicated almost no change in the energy and geometric structure. After finishing the geometry optimizations, the band structures, DOS and PDOS of anatase, rutile and brookite TiO_2 were calculated.

3. Results and discussion

3.1. Electronic properties

The conventional unit cells of anatase, rutile and brookite TiO_2 are shown in Fig. 1. The space groups of anatase, rutile and brookite TiO_2 are $I4_1/amd$, $P4_2/mnm$ and $Pbca$, respectively. The lattice parameters and volumes of anatase, rutile and brookite TiO_2 obtained from the DFT calculation and experiment results are summarized in Table 1. The deviations between calculated and experimental values all are less than 3%, which is consistent with the reliability of present DFT calculations.

To clarify the underlying electronic properties of the anatase, rutile and brookite TiO_2, the DOS and band structures of anatase, rutile and brookite TiO_2 are shown in Fig. 2a–c, respectively. The constitutions of DOS in anatase, rutile and brookite are similar (see Fig. 2). The valence bands primarily consist of O 2p states and a few Ti 3d states, indicating the strong p–d hybridizations

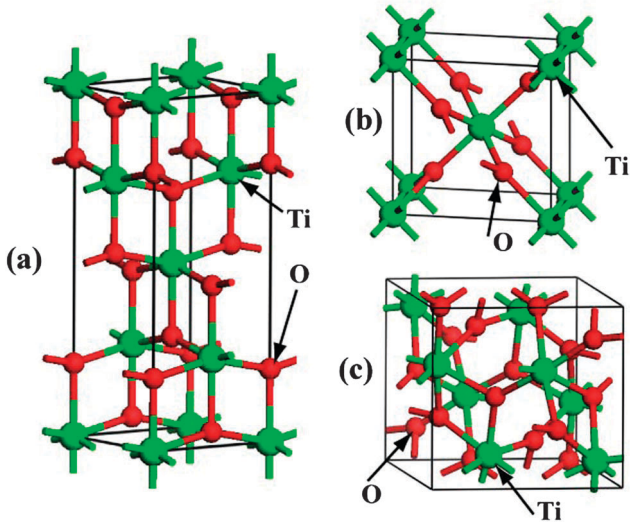

Fig. 1 The schematic conventional cells for anatase (a), rutile (b) and brookite (c) TiO_2. The big green spheres represent Ti atoms and the small red spheres represent O atoms.

Table 1 The optimized lattice parameters and relative deviations for anatase, rutile and brookite TiO_2

Species	Parameter	*a* (Å)	*b* (Å)	*c* (Å)	*V* (Å^3)	$\alpha = \beta = \gamma$ (°)
Anatase	Exp[a]	3.796	3.796	9.444	136.084	90
	DFT	3.800	3.800	9.700	140.068	90
	Deviation/%	0.1	0.1	2.7	3.0	0
Rutile	Exp[b]	4.602	4.602	2.956	62.603	90
	DFT	4.643	4.643	2.965	63.918	90
	Deviation/%	0.9	0.9	0.3	2.1	0
Brookite	Exp[c]	9.166	5.436	5.135	255.858	90
	DFT	9.257	5.501	5.177	263.627	90
	Deviation/%	1.0	1.2	0.8	3.0	0

[a] Ref. 24. [b] Ref. 25. [c] Ref. 26.

between O 2p and Ti 3d states, which form bonding states in the valence band region. Furthermore, the hybridizations broaden the valence bands and promote the transfer of photogenerated holes.[27] Moreover, the conduction bands are mainly composed by Ti 3d states, mixed with a few O 2p and Ti 3p states. In the conduction bands, strong hybridization also appears between Ti 3d and O 2p states, which results in the formation of the anti-bonding states.

The energy band structures of anatase, rutile and brookite TiO_2 along the high symmetry directions in the Brillouin zone were calculated. The Fermi level, shown by a dashed line in Fig. 2, is set as zero. For anatase, an indirect band gap of 2.13 eV was observed between the conduction band minimum (CBM) at G point and the valence band maximum (VBM) at B point along the ZM direction. The rutile and brookite belong to direct band gap semiconductor category and their corresponding band gaps are 1.86 and 2.38 eV at G point, respectively. The calculated band gaps are similar to the previous reported results.[28,29] It should be noted that these values are much smaller than the experimental values (3.2 for anatase, 3.0 for rutile and 3.3 eV for brookite, respectively).

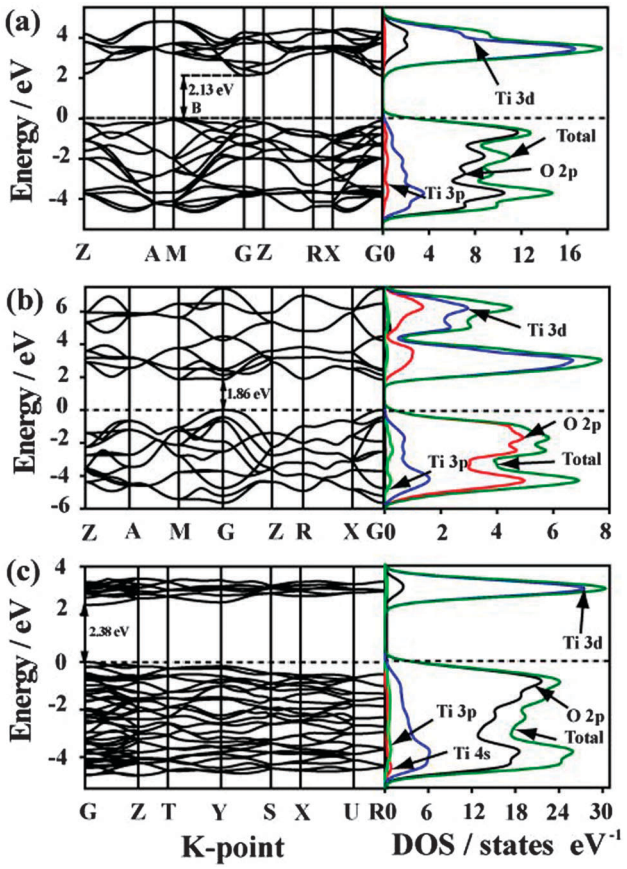

Fig. 2 The band structure and DOS for anatase (a), rutile (b) and brookite (c) TiO_2.

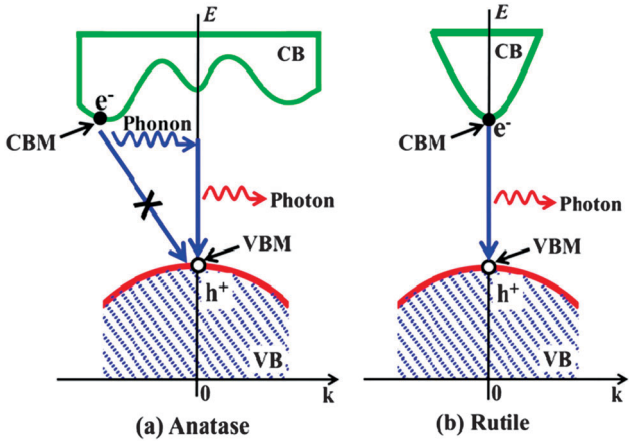

Fig. 3 Comparison of recombination processes of photogenerated electrons and holes within indirect gap anatase (a) and direct gap rutile (b).

This is owing to the well-known shortcoming of the GGA function in DFT calculations.[8,30]

When the excited electrons come back from the conduction band to the valence band due to the recombination of photogenerated electrons and holes, they will release their extra energy as photons. Moreover, the excited electrons must meet the transition selection rule of momentum conservation, which can be illustrated by the following formulae:

$$E_g = \hbar\omega_{\text{photon}} \quad (1)$$

$$\hbar k_e' - \hbar k_e = \pm\hbar q_{\text{phonon}} \quad (2)$$

where $\hbar$ is the reduced Planck constant, k_e' and k_e are the electron wave vectors at the VBM and CBM, respectively, q_{phonon} is the wave vector of the assisted phonon, E_g is the band gap of semiconductor, and ω_{photon} is angular frequency of the emissive photon. For rutile and brookite, an electron only emits a photon for the recombination of photogenerated charge carrier because $k_e' = k_e$ for the direct band gap semiconductors. However, the recombination of photoexcited electron and hole in anatase is assisted by phonon due to $k_e' \neq k_e$ for the indirect band gap semiconductors. Thus, the excited electrons cannot recombine directly with holes, resulting in an increase of the photogenerated electron–hole lifetime in anatase relative to that of rutile and brookite. Fig. 3 shows the indirect band gap of anatase making direct recombination of photogenerated electrons from CBM with holes from VBM impossible, thus increasing the electron–hole lifetime relative to direct band gap of rutile. As a result, the diffusion length and reaction time of the electron and hole excited in the anatase also increase. This is one of the reasons why the indirect semiconductor usually has better photocatalytic performance than direct semiconductor in most reports.

3.2. Effective mass of electron and hole

The quantum efficiency of photocatalyst is also affected by the transfer rate of photogenerated electrons and holes. The transfer rate of charge carriers can be indirectly assessed by the effective mass of electrons and holes,[20,31] which can be explained in the following formula:

$$v = \hbar k/m^* \quad (3)$$

where m^* is the effective mass of the charge carrier, k is the wave vector, $\hbar$ is the reduced Planck constant, and v is transfer rate of photogenerated electrons and holes.

Generally, the transfer rate of photogenerated electrons and holes is inversely proportional to their effective masses; *i.e.*, the larger is the effective mass of photogenerated carriers, the slower is the transfer rate of carriers. Thus, the small effective mass can promote the migration of charge carriers and inhibit the recombination of charge carriers. In order to explain the difference of photocatalytic performance among anatase, rutile and brookite phases TiO_2, the effective mass of electrons (m_e^*) and holes (m_h^*) along designated directions were calculated by fitting parabolic functions around the CBM or the VBM according to the following equations:

$$m^* = \hbar^2\left(\frac{d^2E}{dk^2}\right)^{-1} \quad (4)$$

where m^* is the effective mass of the charge carrier, k is the wave vector, $\hbar$ is the reduced Planck constant, and E is the energy of an electron at wavevector k in that band. To acquire the validity of the parabolic approximation within the CBM and VBM regions, the region for parabolic fitting is within an energy

Table 2 The effective mass of electrons and holes for anatase, rutile, and brookite TiO_2 obtained from parabolic fitting to the CBM and VBM along a specific direction in the reciprocal space

Species		m_e^*/m_0		m_h^*/m_0	
Anatase	Direction	G → Z	G → M	B → G	B → M
	Calculation	0.1412	0.0484	0.2028	0.1961
	Average	0.0948		0.1995	
Rutile	Direction	G → Z	G → M	G → Z	G → M
	Calculation	0.1284	0.0614	1.0018	0.1221
	Average	0.0949		0.5620	
Brookite	Direction	G → Z		G → Z	
	Calculation	1.4610		0.4345	

difference of 1 meV in a particular direction around the CBM or VBM. This method is also used by Ma *et al.* to calculate the effective mass of carriers for silver halide-based Ag@AgX (X = Cl, Br, I).[32] The obtained results are summarized in Table 2.

Chen and co-workers reported that the minimum effective mass of photogenerated electrons and holes in $CaZrTi_2O_7$ are about $1.35m_0$ and $1.23m_0$, respectively.[33] Furthermore, Liu *et al.* also calculated the minimum effective mass of photogenerated electrons and holes in $NaBiO_3$ to be about $0.14m_0$ and $1.10m_0$, respectively.[34] Compared with the reported results, the effective mass of carriers in the anatase and rutile TiO_2 is smaller than that of carriers in $CaZrTi_2O_7$ and $NaBiO_3$. This also explains why anatase and rutile TiO_2 have higher photocatalytic activity than $CaZrTi_2O_7$ and $NaBiO_3$ due to its lighter effective mass. Furthermore, observation from Table 2 indicates that the average effective mass of photogenerated electrons and holes in anatase is smaller than that of rutile and brookite, indicating the transfer rate of the holes and electrons in anatase is the fastest among the three materials. This indicates that the photoexcited charge carriers of anatase more easily migrate and transfer to the surface from its interior to participate in photocatalytic reactions due to its lighter effective mass and smaller particle size. This is illustrated by Fig. 4. Therefore, it is easy to understand why anatase TiO_2 shows better photocatalytic performance than rutile and brookite.

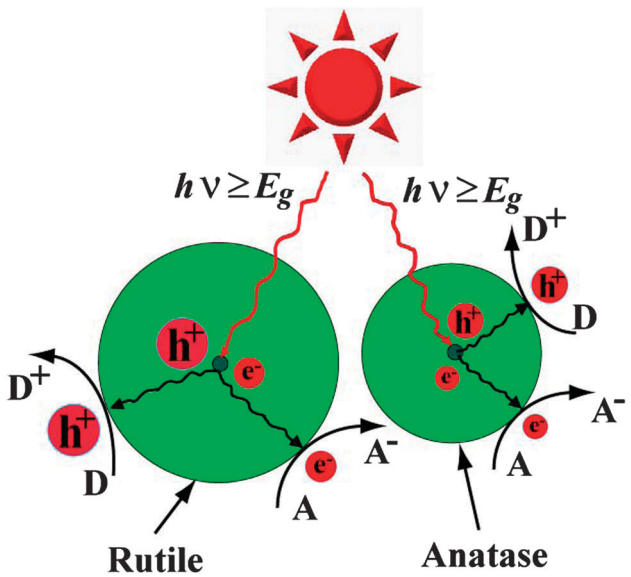

Fig. 4 Transfer diagram of photogenerated electrons and holes for anatase and rutile TiO_2. The bigger green sphere represents larger rutile particle and the small green sphere represents smaller anatase particle. The sizes of red sphere areas represents the differences in effective mass of electrons and holes.

4. Conclusions

The plane-wave pseudopotential method was applied to calculate the electronic structures and charge carrier effective mass of anatase, rutile and brookite TiO_2. The calculation results show that band gaps of anatase, rutile and brookite are 2.13, 1.86 and 2.38 eV, respectively. Anatase is an indirect band gap semiconductor. In contrast, both rutile and brookite belong to the direct band gap semiconductor category. This leads to the lifetime of photogenerated electrons and holes in anatase being longer than that of rutile and brookite. The valence bands of anatase, rutile and brookite are mainly composed of O 2p states, which are mixed with a few Ti 3d states. Above the Fermi level, the conduction bands consist of Ti 3d states, with a small amount of O 2p and Ti 3p states. The calculated average effective mass of electrons and holes in anatase is smaller than that of rutile and brookite. The smaller effective mass of photogenerated charge carriers can facilitate their migration and improve photocatalytic activity. Due to anatase having a lighter effective mass, smaller particle size and longer lifetime of photoexcited electrons and holes, it is not surprising that anatase has a higher photocatalytic performance than rutile and brookite. Therefore, the present studies will provide new insight into the fundamental understanding on photocatalytic mechanism and performance enhancement.

Acknowledgements

This work was supported by the 973 project (2013CB632402) and NSFC (51272199, 51320105001, 51372190 and 21177100). Moreover, this work was financially supported by the Fundamental Research Funds for the Central Universities (2014-VII-010) and the Self-determined and Innovative Research Funds of SKLWUT (2013-ZD-1).

Notes and references

1 M. R. Hoffmann, S. T. Martin, W. Choi and D. W. Bahnemannt, *Chem. Rev.*, 1995, **95**, 69.
2 M. A. Fox and M. T. Dulay, *Chem. Rev.*, 1993, **93**, 341.
3 G. P. Dai, J. G. Yu and G. Liu, *J. Phys. Chem. C*, 2011, **115**, 7339.
4 Q. J. Xiang, J. G. Yu and M. Jaroniec, *Chem. Soc. Rev.*, 2012, **41**, 782.
5 A. Fujishima and K. Honda, *Nature*, 1972, **238**, 37.
6 J. F. Reber and M. Rusek, *J. Phys. Chem.*, 1986, **90**, 824.
7 Q. J. Xiang, J. G. Yu and M. Jaroniec, *J. Am. Chem. Soc.*, 2012, **134**, 6575.
8 Q. Tay, X. Liu, Y. Tang, Z. Jiang, T. C. Sum and Z. Chen, *J. Phys. Chem. C*, 2013, **117**, 14973.

9 A. Beltran, L. Gracia and J. Andres, *J. Phys. Chem. B*, 2006, **110**, 23417.
10 M. Xu, Y. Gao, E. M. Moreno, M. Kunst, M. Muhler, Y. Wang, H. Idriss and C. Woll, *Phys. Rev. Lett.*, 2011, **106**, 138302.
11 A. L Linsebigler, G. Q. Lu and J. T. Yates, *Chem. Rev.*, 1995, **95**, 735.
12 J. G. Li, T. Ishixaki and X. Sun, *J. Phys. Chem. C*, 2007, **111**, 4969.
13 J. G. Yu, J. C. Yu, M. K. P. Leung, X. J. Zhao, W. K. Ho and J. C. Zhao, *J. Catal.*, 2003, **217**, 69.
14 D. A. H. Hanaor and C. C. Sorrell, *J. Mater. Sci.*, 2010, **46**, 855.
15 A. Sclafani and J. M. Herrmann, *J. Phys. Chem.*, 1996, **100**, 13655.
16 Q. Zhang, L. Gao and J. Guo, *Appl. Catal., B*, 2000, **26**, 207.
17 Z. Zhang, C. C. Wang, R. Zakaria and J. Y. Ying, *J. Phys. Chem. B*, 1998, **102**, 10871.
18 J. M. Kesselman, G. A. Shreve, M. R. Hoffmann and N. S. Lewis, *J. Phys. Chem.*, 1994, **98**, 13385.
19 N. Umezawa, O. Shuxin and J. Ye, *Phys. Rev. B: Condens. Matter Mater. Phys.*, 2011, **83**, 1.
20 J. G. Yu, P. Zhou and Q. Li, *Phys. Chem. Chem. Phys.*, 2013, **15**, 12040.
21 M. D. Segall, P. J. D. Lindan, M. J. Probert, C. J. Pickard, P. J. Hasnip, S. J. Clark and M. C. Payne, *J. Phys.: Condens. Matter*, 2002, **14**, 2714.
22 J. P. Perdew, K. Burke and M. Ernzerhof, *Phys. Rev. Lett.*, 1996, **77**, 3865.
23 J. P. Perdew and Y. Wang, *Phys. Rev. B: Condens. Matter Mater. Phys.*, 1992, **45**, 13244.
24 M. Horn, C. F. Schwerdtfeger and E. P. Meagher, *Z. Kristallogr.*, 1972, **136**, 273.
25 T. M. Sabine and C. J. Howard, *Acta Crystallogr., Sect. B: Struct. Crystallogr. Cryst. Chem.*, 1982, **38**, 701.
26 E. P. Meagher and G. A. Lager, *Can. Mineral.*, 1979, **17**, 77.
27 J. J. Liu, X. L. Fu, S. F. Chen and Y. F. Zhu, *Appl. Phys. Lett.*, 2011, **99**, 191903.
28 C. D. Valentin, G. Pacchioni and A. Selloni, *Chem. Mater.*, 2005, **17**, 6656.
29 H. Kamisaka, T. Adachi and K. Yamashita, *J. Chem. Phys.*, 2005, **123**, 084704.
30 J. P. Perdew and L. Mel, *Phys. Rev. Lett.*, 1983, **51**, 1884.
31 P. Zhou, J. G. Yu and Y. X. Wang, *Appl. Catal., B*, 2013, **142–143**, 45.
32 X. C. Ma, Y. Dai, M. Guo and B. B. Huang, *ChemPhysChem*, 2012, **13**, 2304.
33 J. J. Liu, S. Chen and Y. F. Zhu, *Solid State Commun.*, 2012, **152**, 1650.
34 J. J. Liu, S. F. Chen, Q. Z. Liu, Y. F. Zhu and J. F. Zhang, *Chem. Phys. Lett.*, 2013, **572**, 101.

